NUMERICAL SIMULATION ON THE HIGH VELOCITY IMPACT DAMAGE IN THE CFRP LAMINATES

A. Yoshimura[1], K. Ogi[2], T. Ogasawara[1], H. Sasaki[3], K. Miyoshi[2]

[1] Japan Aerospace Exploration Agency, 6-13-1 Osawa, Mitaka, Tokyo 181-0015, Japan,
email: yoshimura.akinori@jaxa.jp
[2]Ehime University, 3 Bunkyo-cho, Matsuyama, Ehime 790-8577, Japan
[3]Toray Industries, Inc., 1515 Tsutsui, Matsumae-cho, Iyo-gun, Ehime 791-3193, Japan

SUMMARY

This paper proposes a numerical model that simulates the high velocity impact damage in the CFRP. Fiber failure, ply cracks, and delamination are modelled by stress criterion, continuum damage mechanics, and cohesive zone model. Experimental and simulation results demonstrate the proposed model successfully simulates damage process in the CFRP.

Keywords: High velocity impact, CFRP, Numerical simulation, Finite element analysis, Continuum damage mechanics

INTRODUCTION

Since global environmental problems are growing more serious, the dramatic decreasing of the environmental load is an essential issue for the next generation aircraft. Therefore the development of more energy-efficient turbofan engines is strongly demanded. Structural weight reduction is effective to increase the energy-efficiency. Advanced composite group in Japan Aerospace Exploration Agency (JAXA) is conducting basic researches on the application of composite materials to the structures of turbofan engines.

The present focus of the study is the application of CFRP laminates to the fan system, fan blades and a fan case. Fan blades are at forefront of the engine, and the blades often experience the collisions of the foreign objects such as birds. The foreign object impact might cause the fracture of fan blades, and broken pieces of blades might conflict against the fan case. Fan case must sustain the collision of the broken pieces. The impact velocity of foreign objects against the fan blades is approximately equal to total of cruise speed and rotation speed of the blades. And the collision velocity of broken pieces against the fan case is approximately equal to the rotation speed of the tip of the blade. In both events, the impact velocity ranges from 100 to 500 m/s. Hence, for application to fan system, it is quite important to investigate the high velocity (~500m/s) impact properties of CFRP laminates. Especially, precise prediction of ballistic limit of CFRP laminates is essential.

Some researchers have conducted the high velocity impact tests against the CFRP laminates[1-4]. Among them, Tanabe et al.[4] performed high velocity impact tests for

composites which have various reinforcing fibers and have various properties of interface between fibers and matrix. They found that the material properties of reinforcing fibers and the properties of interface strongly affect the ballistic limits of the composite materials.

Under high velocity impact load, damage, such as ply cracks, delamination and fiber failure, occurs and propagates in CFRP laminates. The fact that not only properties of reinforcing fibers but also interface properties affect the ballistic limit implies that occurrence and evolution of damage strongly affect the kinetic energy absorption of CFRP laminates. Hence, in order to predict the ballistic limit of CFRP laminate precisely, it is essential to predict the damage occurrence and propagation in CFRP. However, the analysis of damage occurrence and propagation has not been studied sufficiently.

The goal of present study is to establish the scheme for prediction of damage occurrence, damage propagation, and ballistic limit of CFRP laminates. In the present paper, the simple finite element analysis model for damage simulation of CFRP laminates is proposed, and the verification of model is conducted by comparing the simulation results to experimental results. The present paper is organized as follows. In section 2, high velocity impact tests are conducted, and the experimental observation of damage is briefly described. In section 3, the finite element model is formulated, then we conduct the finite element analyses, and the results are compared to the experimental results.

EXPERIMENTAL

Experimental Procedure

We conducted high velocity impact tests for two types of CFRP laminates. Every prepreg was fabricated by Toho Tenax Co. Ltd. Stacking sequence was $[0/90]_{4s}$ in both specimens. High strength PAN carbon fiber IMS60 was used for reinforcing fiber. For matrix resin, #133 resin was used for specimens type A, but #132 was used for type B. #133 and #132 are both epoxy resin, but #133 is tougher than #132.

The dimensions of specimen were shown in Fig. 1, 102 mm in length direction, and 76 mm in width direction. Thickness of specimens are about 2.2 mm. Specimens were fixed by picture frame type fixture. Specimen was placed between the base plate and holder plate. The base plate had recutangularly shaped window; the dimensions were 80 mm in length direction and 60 mm in width direction. Holder plate also had rectangularly shaped window; the dimensions were 97 mm x 71 mm. The holder plate was lightly clamped to the base plate with four bolts.

Spherical projectile of diameter of 6.0 mm collided at the center of the specimen. The projectile was made of bearing steel, weight of which was about 0.88 g. A projectile was supported by sabot, and was accelerated by high pressure plasma, which was generated by evaporation of aluminium foil by high voltage impulse current. The impact velocity was measured by built-in speed detector.

After the impact tests, two kinds of soft X-ray NDI were conducted for detailed observation of the impact damage. We took soft X-ray radiographs by using general purpose soft X-ray film device (SV-100AW, SOFTEX, Inc.) in order to observe the in-plane distribution of the damage. In addition, we took section images by soft X-ray

micro-focus Computed Tomography (CT) system (TOSCANER-30000μhd, TOSHIBA IT & Control Systems Corp.) in order to observe through-the-thickness distribution of the damage.

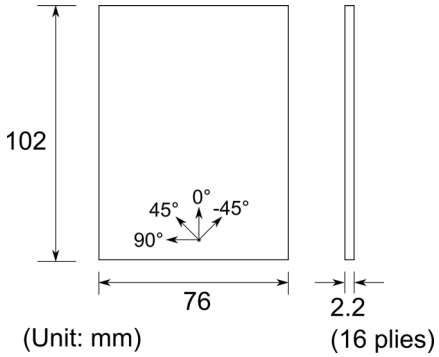

Fig. 1 Dimensions of the specimen

Experimental Results

Surface impact damage was shown in Fig. 2. Measured projectile velocity was 180 m/s in specimen A, and 140 m/s in specimen B. In both specimen A and B, projectile penetration did not occur. At obverse surface, the projectile collision generated crater. On the other hand at reverse surface, several long straight cracks occurred along 0° direction.

Figure 3 shows soft X-ray radiographs of the specimens. Although impact velocity of specimen B was lower than that of specimen A, we clearly see the greater damage area in specimen B. Impact damage spread along the 0° direction. By comparing Fig. 2 and Fig. 3, we concluded that the delamination spread near the bottom of the specimen along the cracks on the bottom surface.

Figure 4 shows micro-focus X-ray CT images. The damage profile in thickness direction was similar to the low velocity impact damage. In both specimens, delamination became gradually greater from the top to the bottom of the specimen, and there was the greatest delamination occurred at the bottom of the specimen. Ply cracks connected the delamination. Delamination occurred more interfaces in the specimen B than in the specimen A.

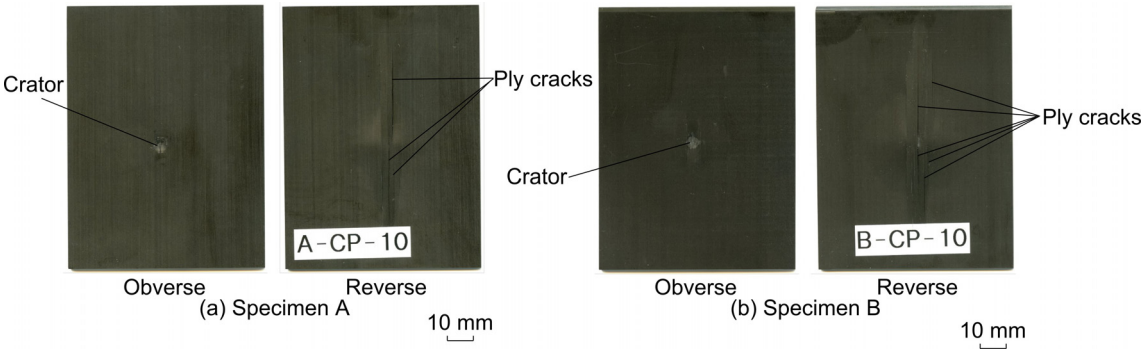

Fig 2. Surfaces damages of the specimens

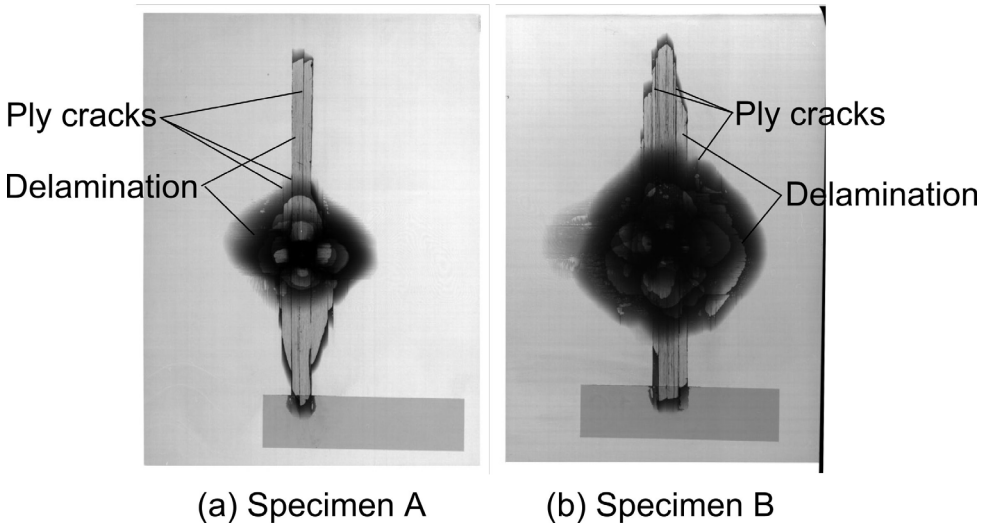

Fig. 3 Xray radiographs of the specimens

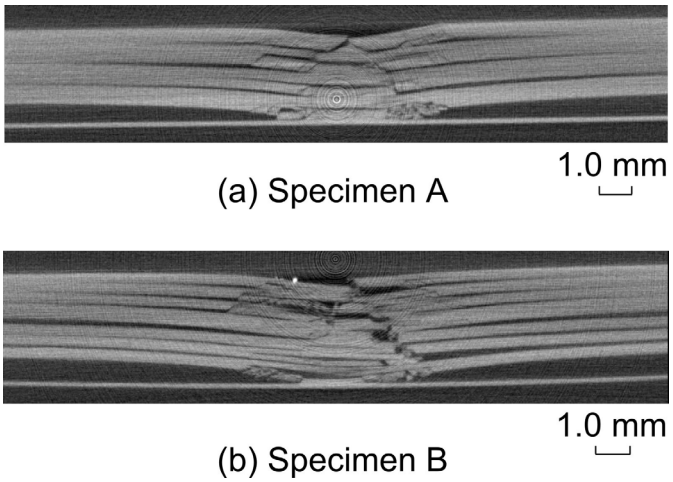

Fig. 4 Xray CT images of the specimens

ANALYSIS

Damage Modelling

We conducted finite element analysis in order to simulate damage process in the CFRP laminate. In the analysis, three types of damage were considered; fiber failure, ply cracks, delamination. In this section, formulations of fiber failure and ply cracks in single ply are described first, then the formulation of delamination is described.

We considered fiber tensile and compressive failure by degradation of the material properties of the brick element. We determined fiber failure by simple stress criterion. Tensile and shear failure was determined by

$$\left(\frac{\langle \sigma_1 \rangle}{S_L^{\ T}}\right)^2 + \left(\frac{\tau_{13}}{S_{LT}}\right)^2 = 1 \tag{1}$$

where subscript L denotes fiber direction, T denotes thickness direction (see Fig. 5), ${S_L}^T$ means tensile strength in fiber direction, S_{LT} means shear strength. The angle bracket means $\langle x \rangle = 0$ when $x < 0$, and $\langle x \rangle = x$ when $x \geq 0$. The failure was determined at integration point of element, and the element where fiber tensile failure occurred was immediately vanished. On the other hand, fiber compressive failure was determined by

$$\left(\frac{\langle -\sigma_1 \rangle}{{S_L}^C} \right) = 1 \tag{2}$$

where ${S_L}^C$ is compressive strength. The element where fiber compressive failure occurred was not vanished, but stiffness in fiber direction was set to close to zero.

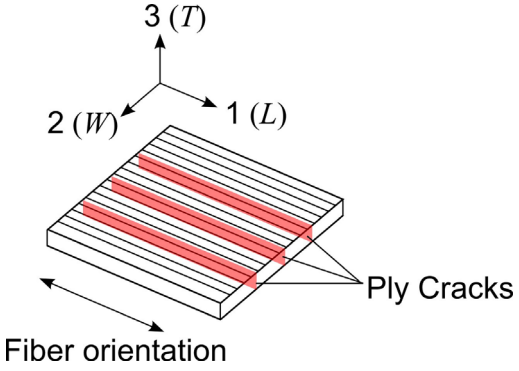

Fig. 6 Fiber orientation and coordinates in single ply formulation

Transverse ply cracks were modelled by using continuum damage mechanics[5,6]. In the usual formulation of the continuum damage mechanics, one defines effective stress, which means the stress enlarged by distributed damage. However, in this study, authors used effective strain $\tilde{\boldsymbol{\varepsilon}}$, which was defined by

$$\tilde{\boldsymbol{\varepsilon}} = \frac{1}{2}\left[(\boldsymbol{I} - \boldsymbol{D})\boldsymbol{\varepsilon} + \boldsymbol{\varepsilon}(\boldsymbol{I} - \boldsymbol{D}) \right] \tag{3}$$

where $\boldsymbol{\varepsilon}$ is strain tensor, $\boldsymbol{I}$ is unit tensor, and $\boldsymbol{D}$ is damage tensor. If the crack occurred parallel to the 1 direction (see Fig. 5), Damage tensor $\boldsymbol{D}$ is expressed as

$$\boldsymbol{D} = d_2 \, \boldsymbol{n}_2 \otimes \boldsymbol{n}_2 \tag{4}$$

where d_2 is damage parameter. When there is no damage, d_2=0, and d_2 grows up to 1 as damage evolves. $\boldsymbol{n}_2$ is unit vector, the direction of which is parallel to the 2 direction. By using effective strain, we can calculate the stress as

$$\boldsymbol{\sigma} = \boldsymbol{C}\tilde{\boldsymbol{\varepsilon}} = \frac{1}{2}\boldsymbol{C}\left[(\boldsymbol{I} - \boldsymbol{D})\boldsymbol{\varepsilon} + \boldsymbol{\varepsilon}(\boldsymbol{I} - \boldsymbol{D}) \right] \tag{5}$$

where $\boldsymbol{C}$ is the stiffness matrix of the material which does not contain damage. By using equations (4) and (5), strain energy e is calculated as

$$e=\frac{1}{2}\Big[C_{11}{\varepsilon_{11}}^2+(2-d_2)C_{12}\varepsilon_{11}\langle\varepsilon_{22}\rangle+2C_{12}\varepsilon_{11}\langle-\varepsilon_{22}\rangle+2C_{13}\varepsilon_{11}\varepsilon_{33}+(1-d_2)C_{22}\langle\varepsilon_{22}\rangle^2+$$
$$C_{22}\langle-\varepsilon_{22}\rangle^2+(2-d_2)C_{23}\langle\varepsilon_{22}\rangle\varepsilon_{33}+2C_{23}\langle-\varepsilon_{22}\rangle\varepsilon_{33}+C_{33}{\varepsilon_{33}}^2+(1-d_2/2)C_{44}\gamma_{12}+ \quad (6)$$
$$C_{55}{\gamma_{13}}^2+(1-d_2/2)C_{66}{\gamma_{23}}^2\Big]$$

where C_{xy} means xy components of stiffness matrix. Damage force Y_2=-($\partial e/\partial d_2$) can be obtained as

$$Y_2=\frac{1}{2}\left[C_{12}\varepsilon_{11}\langle\varepsilon_{22}\rangle+C_{22}\langle\varepsilon_{22}\rangle^2+C_{23}\langle\varepsilon_{22}\rangle\varepsilon_{33}+\frac{1}{2}C_{44}{\gamma_{12}}^2+\frac{1}{2}C_{66}{\gamma_{23}}^2\right] \quad (7)$$

Note that d_2 does not appear in the calculation of Y_2. We obtained damage evolution function, namely, d_2-Y_2 relationship from the tensile test of cross-ply laminate [7] (see Fig. 6). During calculation, Y_2 is calculated by using strain, and from Y_2-d_2 relationship we obtain d_2, and stress is updated by using equation (5).

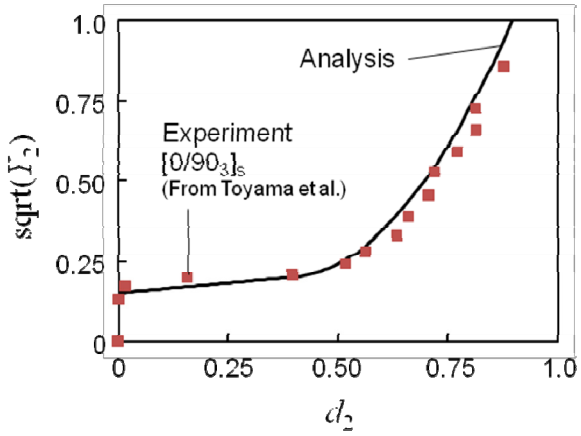

Fig. 6 d_2-Y_2 relationship

We employed cohesive elements in order to simulate the delamination. A cohesive element is the cohesive zone model, which is introduced between two brick elements. The cohesive element generates the cohesive traction that resists the increase of the relative displacement between the brick elements. The cohesive element behaves as the penalty spring when the relative displacement is so small. After cohesive traction reaches threshold value, cohesive traction gradually decreases, and vanishes. Until then, a cohesive element absorbs the energy which is equal to fracture toughness.

Finite Element Model

Figure 7 illustrates the numerical analytical model used in this study. Stacking sequence was $[0/90]_{4s}$, which is same as that of the specimen used in section 2. Considering the symmetries in x and y direction, only a quarter of the specimen was modeled. The thickness of the model was 2.2 mm. Linear reduced integration eight-node brick elements expressed the laminate, and one ply was modeled by two elements. The material properties of the brick elements were calculated by the equations described in section 3. Too distorted elements (any one component of strain exceeded 30%) and the elements judged as fiber failure were vanished.

The projectile was modelled by rigid surface. Fixture was also modeled by rigid surface. The hard contacts were considered between the laminates and projectile, laminates and fixture, while the friction was not considered.

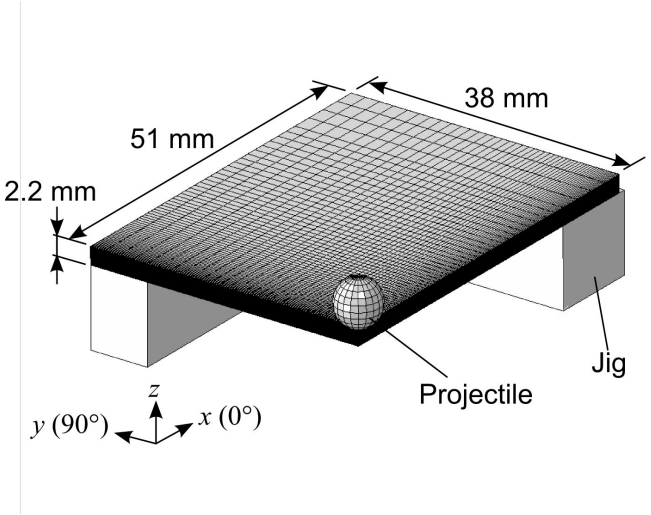

Fig. 7 Overview of the analytical model

Analytical Results

For calculation, general-purpose commercial FEA code, ABAQUS explicit 6.8-3 was employed. The formulations of fiber failure and ply cracks were implemented by using user subroutine vumat. For delamination, built-in cohesive elements were used. In this study, initial velocity of the projectile was set to 150 m/s. The material properties and the properties of cohesive elements are shown in Table 1 and 2.

Table 1 Material properties used in the analysis

Longitudinal Young's modulus E_1 (MPa)	165
Transverse Young's modulus E_2, E_3(MPa)	7.73
Longitudinal Poisson's ratio ν_{12}, ν_{13}	0.326
Transverse Poisson's ratio ν_{23}	0.450
Longitudinal shear modulus G_{12}, G_{13} (MPa)	3.83
Transverse shear modulus G_{23} (MPa)	3.40
Tensile strength S_L^T (MPa)	1000
Compressive strength S_L^C (MPa)	785
Shear strength S_{LT} (MPa)	300

Table 2 Properties of cohesive elements used in the analysis

Mode I threshold traction σ_{max} (MPa)	65
Mode II threshold traction τ_{max} (MPa)	150
Mode III threshold traction τ_{max} (MPa)	150
Mode I fracture toughness G_{Ic} (J/m^2)	435
Mode II fracture toughness G_{IIc} (J/m^2)	1855
Mode III fracture toughness G_{IIIc} (J/m^2)	1855

Figure 8 shows the damage parameter d_2. Figure 9 shows delamination growth. Delamination, ply cracks and fiber failure propagated with influence on each other. On the obverse surface of the model, projectile collision caused fiber tensile failure, which generated crater on the surface. At the reverse surface, ply damage area, in which d_2 was large, spread along 0° direction. Delamination area became greater from the top to the bottom of the model. Largest delamination occurred near the bottom of the model. These features agreed well with the experimental observation qualitatively. These results demonstrated that although the proposed numerical analytical model was simple, it successfully simulated the damage process of the high velocity impact.

CONCLUSION

In the present paper, the simple finite element analysis model for damage simulation of CFRP laminates was proposed, and the verification of model was conducted by comparing the simulation results to experimental results. The analytical model was based on the finite element model, which included the cohesive elements and the continuum damage mechanical model. The comparison of simulation results and experimental observation demonstrated that the model successfully simulated the high velocity impact damage process in CFRP laminates.

ACKNOWLEDGEMENTS

Dr. Tomonaga Okabe in Tohoku University gave us many useful advices about the formulation of the numerical model. Authors sincerely appreciate his advices.

References

1. J. Lopez-Puente, R. Zaera and C. Navarro: “An analytical model for high velocity impacts on thin CFRPs woven laminated plates,” *Int. J. Solid. Struct.*, 44, 2837-2851 (2007).
2. J. Lopez-Puente, R. Zaera and C. Navarro, “Experimental and numerical analysis of normal and oblique ballistic impacts on thin carbon/epoxy woven laminates,” *Composites Part A*, 39A, 374-387 (2008).

3. G. Caprino, V. Lopresto and D. Santoro, “Ballistic impact behavior of stitched graphite/epoxy laminates,” *Compos. Sci. Technol.*, 67, 325-335 (2007).

4. Y. Tanabe, M. Aoki, K. Fujii, H. Kasano and E. Yasuda, “Fracture behavior of CFRPs impacted by relatively high-velocity steel sphere,” *Int. J. Impact Eng.*, 28, 627-642 (2003).

5. J. Skrzypek and A. Ganczarski, “Modeling of Material Damage and Failure of Structures,” Springer, Berlin, 1999.

6. G. Lubineau and P. Ladevèze, “Construction of a micromechanics-based intralaminar mesomodel, and illustrations in ABAQUS/Standard,” *Comput. Mater. Sci.*, 43, 137-145 (2008).

7. N. Toyamaa, J. Noda and T. Okabe, “Quantitative damage detection in cross-ply laminates using Lamb wave method,” *Compos. Sci. Technol.*, 63, 1473-1479 (2003).

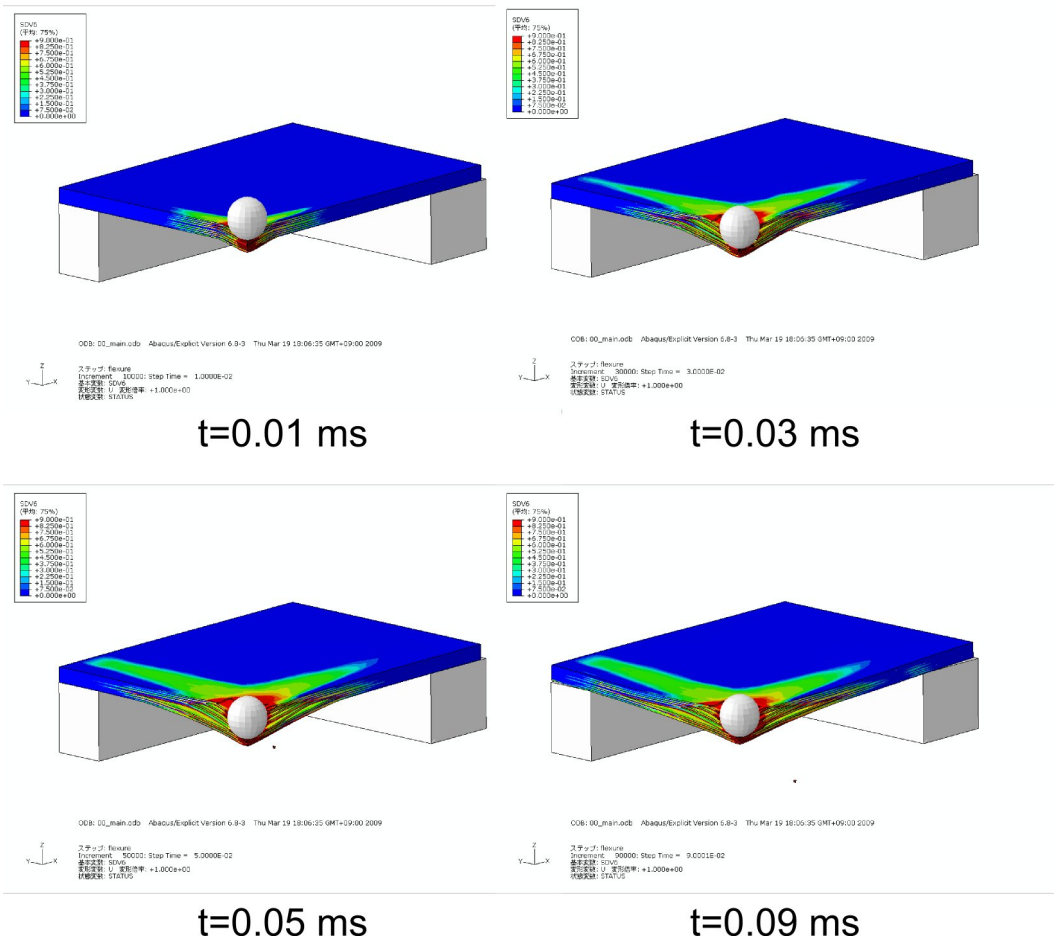

Fig. 8 Distribution of damage parameter d_2 during calculation

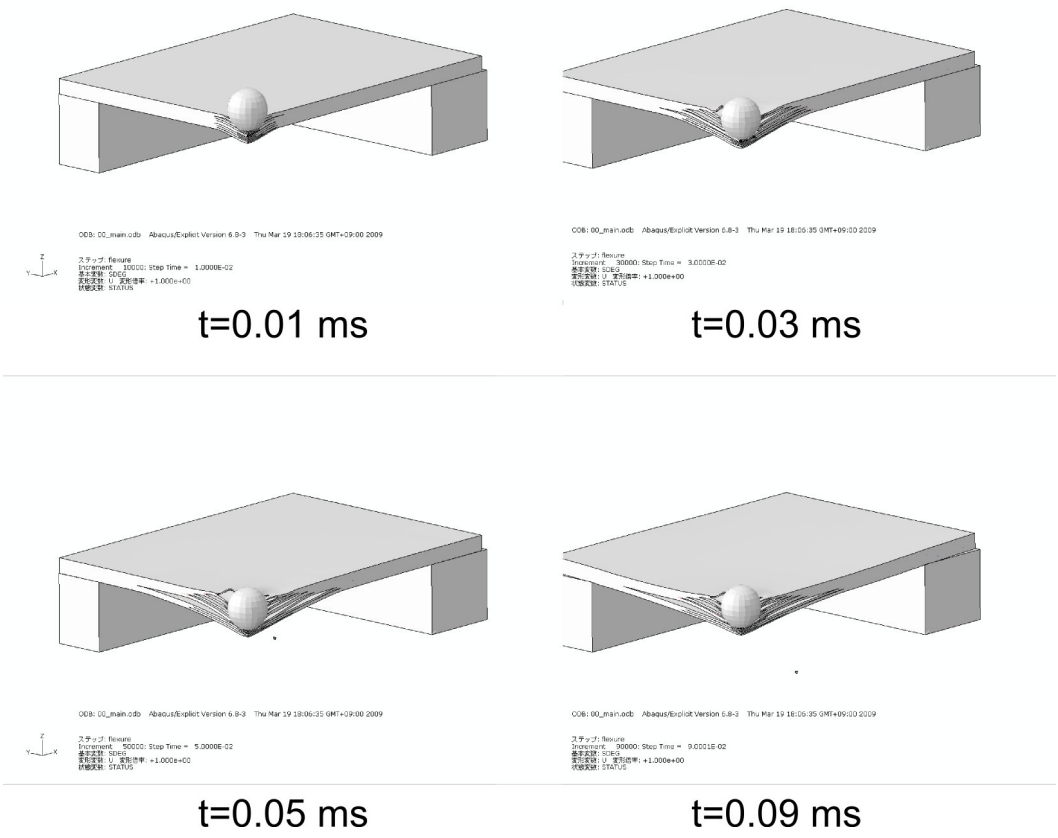

Fig. 9 Delamination extension during calculation

Previous Paper ***Back to Programme*** ***Back to Topic*** *Next Paper*